

Low-temperature dynamics of weakly localized Frenkel excitons in disordered linear chains

M. Bednarz

Institute for Theoretical Physics and Materials Science Center, University of Groningen, Nijenborgh 4, 9747 AG Groningen, The Netherlands

V. A. Malyshev

S.I. Vavilov State Optical Institute, Birzhevaya Liniya 12, 199034 Saint-Petersburg, Russia and Institute for Theoretical Physics and Materials Science Center, University of Groningen, Nijenborgh 4, 9747 AG Groningen, The Netherlands

J. Knoester^{a)}

Institute for Theoretical Physics and Materials Science Center, University of Groningen, Nijenborgh 4, 9747 AG Groningen, The Netherlands

(Received 29 September 2003; accepted 1 December 2003)

We calculate the temperature dependence of the fluorescence Stokes shift and the fluorescence decay time in linear Frenkel exciton systems resulting from the thermal redistribution of exciton population over the band states. The following factors, relevant to common experimental conditions, are accounted for in our kinetic model: (weak) localization of the exciton states by static disorder, coupling of the localized excitons to vibrations in the host medium, a possible nonequilibrium of the subsystem of localized Frenkel excitons on the time scale of the emission process, and different excitation conditions (resonant or nonresonant). A Pauli master equation, with microscopically calculated transition rates, is used to describe the redistribution of the exciton population over the manifold of localized exciton states. We find a counterintuitive nonmonotonic temperature dependence of the Stokes shift. In addition, we show that depending on experimental conditions, the observed fluorescence decay time may be determined by vibration-induced intraband relaxation, rather than radiative relaxation to the ground state. The model considered has relevance to a wide variety of materials, such as linear molecular aggregates, conjugated polymers, and polysilanes.
© 2004 American Institute of Physics. [DOI: 10.1063/1.1643720]

I. INTRODUCTION

The dynamics of excitons in chainlike systems, like conjugated polymers,¹ polysilanes,² and molecular J aggregates,^{3,4} have attracted much attention over recent decades. The dynamics in these systems result from the complicated interplay between various processes, in particular from relaxation to the ground state (population relaxation), from migration of the exciton to sites with different excitation energy (population redistribution), and from relaxation caused by nuclear displacements (exciton self-trapping). Population relaxation is distinguished in radiative and non-radiative channels. With regards to migration, two limiting situations are usually considered. The first one is the case of incoherent energy transfer (Förster transfer), which takes place between strongly localized excitations on the chain. This is also referred to as hopping transfer in a disordered site energy distribution. In the other limit, one deals with weakly localized exciton states, which may extend over many repeat units of the chain. Transitions between such bandlike exciton states are possible due to their scattering on lattice vibrations and are often referred to as intraband relaxation.

The net effect of the above processes may be probed by

various optical techniques, of which steady state and time-resolved fluorescence spectroscopy are the most frequently used ones. Common quantities extracted from such experiments are the decay time of the total fluorescence intensity following pulsed excitation and the steady state as well as the dynamic Stokes shift. As most of the dynamic processes mentioned above are influenced by temperature in a different way, one often also probes the temperature dependence of the fluorescence.

The temperature dependence of the fluorescence decay time has drawn particular attention in the case of molecular J aggregates of polymethine dyes. In these systems, the Frenkel exciton states are delocalized over tens of molecules (weakly localized excitons). The coherent nature of the excitation extended over many molecules leads to states with giant oscillator strengths, which scale like the number of molecules over which the exciton state is delocalized. These so-called superradiant states lie near the bottom of the bare exciton band, and, especially at low temperatures, lead to ultrafast spontaneous emission (tens to hundreds of picoseconds).⁵⁻¹⁴ Upon increasing the temperature, these systems typically exhibit an increase of the fluorescence lifetime, which is a trend that is highly unusual for single-molecule excitations and is intimately related to the extended nature of the exciton states. This temperature dependence

^{a)}Electronic mail: knoester@phys.rug.nl

was first observed for the J aggregates of pseudoisocyanine (PIC),^{5,7,8,10} and later confirmed for other types of J aggregates, in particular, 5,5',6,6'-tetrachloro-1,1'-diethyl-3,3'-di(4-sulfobutyl)-benzimidazolocarboxyanine (TDBC),¹¹ 1,1'-diethyl-3,3'-bis(sulfopropyl)-5,5',6,6'-tetrachlorobenzimidazolocarboxyanine (BIC),¹² and 3,3'-bis(sulfopropyl)-5,5'-dichloro-9-ethylthiacarboxyanine (THIATS).^{14,15} The slowing down of the aggregate radiative dynamics is usually attributed to the thermal population of the higher-energy exciton states, which in J aggregates have oscillator strengths small compared to those of the superradiant exciton states.^{7,8} In spite of the basic understanding that the redistribution of the initial exciton population over the band states plays a crucial role in this problem, the theoretical efforts to describe this redistribution and to fit all details of this behavior have not been fully successful so far^{9,13,16-18} (see Ref. 19). In particular, as we have found from our previous study on homogeneous model aggregates,¹⁹ the initial excitation conditions seem to play a crucial role in the interpretation of the measured fluorescence lifetime: under certain conditions this lifetime probes the intraband relaxation time scale, rather than the superradiant emission time.

The Stokes shift of the fluorescence spectrum in linear exciton systems has been considered previously by various authors; studies of its temperature dependence are rare. One of the first studies concerned the Stokes shift in polysilanes at liquid-helium temperatures, which was modeled in a phenomenological way by assuming that intraband relaxation is determined by one energy-independent relaxation rate in combination with the number of available lower-energy exciton states in a disordered chain.² Relaxation by migration to the lowest-exciton state available on a linear chain also forms the main ingredient of the theoretical study of Chernyak *et al.*²⁰ on the relation between the fluorescence line shape and the superradiant emission rate deep in the red wing of the density of states of disordered J aggregates at cryogenic temperatures. For π -conjugated polymers the time-dependent shift of the luminescence spectrum (dynamic Stokes shift) has been modeled by assuming excitons localized on a few repeat units, which migrate spatially as well as energetically through Förster transfer.²¹⁻²³ It was concluded that the Stokes shift in these systems cannot be explained from nuclear displacements, as would be the case for single molecules, and that the migration process plays a crucial role.²¹ Also for J aggregates, with strongly delocalized exciton states, the belief is that the Stokes shift induced by nuclear displacements is small, in fact much smaller than the Stokes shift of their single-molecule constituents. The explanation lies in the fact that for a delocalized excitation the weight of the excitation on each molecule of the chain is small, which leads to a small nuclear displacement on each molecule. The measured Stokes shift differs for various types of J aggregates, for instance for PIC a shift can hardly be detected,⁶ while for TDBC,¹¹ BIC,¹² and THIATS¹⁵ a clear shift can be observed. As far as we are aware, the temperature dependence of the Stokes shift was only measured for THIATS aggregates.¹⁵ It shows an interesting nonmonotonic behavior, analogous to the one found in disordered narrow quantum wells,²⁴ where it finds its origin in thermally acti-

vated escape from local minima in the random potential.

The goal of this article is to model the temperature dependence of the dynamics of weakly localized excitons in linear chains and to establish the effect on the fluorescence lifetime and Stokes shift. We will be mostly interested in temperatures up to about 100 K, where scattering on acoustic phonons is the dominant scattering mechanism. This article is an extension of our previous work, where we studied the temperature dependence of the fluorescence lifetime and restricted ourselves to ideal (homogeneous) Frenkel chains.¹⁹ Here, we consider a more detailed model, which includes on-site (diagonal) disorder. It is well-known that this model provides a good basis for understanding the complex (linear and nonlinear) optical dynamics in J aggregates.^{7,8,25-29} We will take into account the following factors that seem to be essential under common experimental conditions: (i) localization of the exciton states by the site disorder, (ii) coupling of the localized excitons to the host vibrations (not only to the vibrations of the aggregate itself as was done in Refs. 13 and 16), (iii) a possible nonequilibrium of the subsystem of localized Frenkel excitons on the time scale of the emission process, and (iv) the nature of the excitation conditions (resonant versus nonresonant). We use a Pauli master equation to describe the evolution of the populations of the localized exciton states and the intraband redistribution of population after the initial excitation. Previously, such a master equation was also used to model the exciton dynamics in disordered quantum wells²⁴ and polysilane films.³⁰ As observables, we focus on the Stokes shift of the fluorescence spectrum and the decay times of the total as well as the energy dependent fluorescence intensity.

The outline of this article is as follows: In Sec. II, we present the model Hamiltonian of Frenkel excitons with diagonal disorder, the main effect of which is localization of the exciton states on finite segments of the aggregate. We briefly reiterate the basic facts concerning the structure of the exciton eigenenergies and eigenfunctions close to the band bottom, which is the spectral range that mainly determines the exciton optical response and dynamics. The Pauli master equation that describes the transfer of populations between the various exciton eigenstates, is introduced in Sec. III. The numerical solution of this equation under various conditions is obtained and used in Sec. IV to study the steady-state fluorescence spectra and the temperature dependence of the Stokes shift and in Sec. V to study the temperature dependent fluorescence lifetime. The results are also discussed in terms of back-of-the-envelope estimates based on the low-energy exciton structure. Finally, we summarize and conclude in Sec. VI.

II. DISORDERED FRENKEL EXCITON MODEL

We consider a generic one-dimensional Frenkel exciton model, consisting of a regular chain of N optically active sites, which are modeled as two-level systems with parallel transition dipoles. The corresponding Hamiltonian reads

$$H = \sum_{n=1}^N \epsilon_n |n\rangle \langle n| + \sum_{n,m} J_{nm} |n\rangle \langle m|, \quad (1)$$

where $|n\rangle$ denotes the state in which the n th site is excited and all the other sites are in the ground state. The excitation energy of site n is denoted ϵ_n . We will account for energetic disorder by assuming that each ϵ_n is taken randomly, and uncorrelated from the other site energies, from a Gaussian distribution with mean ϵ_0 and standard deviation σ . Hereafter, ϵ_0 is set to zero. The hopping integrals J_{nm} are considered to be nonrandom, and are assumed to be of dipolar origin: $J_{nm} = -J/|n-m|^3$ ($J_{nn} \equiv 0$). Here, the parameter J represents the nearest-neighbor coupling, which is positive for the systems of our interest, namely those that have the optically dominant states at the bottom of the exciton band. Molecular J aggregates are prototype examples of such systems. Diagonalizing the $N \times N$ matrix $H_{nm} = \langle n|H|m\rangle$ yields the exciton eigenenergies and wave functions. In particular, the ν th eigenvalue E_ν (with $\nu = 1, \dots, N$) is the energy of the exciton state $|\nu\rangle = \sum_{n=1}^N \varphi_{\nu n} |n\rangle$, where $\varphi_{\nu n}$ is the n th component of the ν th eigenvector.

As has been shown in Ref. 31, in the absence of disorder ($\sigma=0$, the case of a homogeneous chain) the eigenvectors in the presence of long-range dipolar interactions with an accuracy of the order of N^{-1} agree with those for the case of nearest-neighbor hopping:

$$|k\rangle = \left(\frac{2}{N+1}\right)^{1/2} \sum_{n=1}^N \sin(Kn) |n\rangle, \quad (2)$$

where we introduced the wave number $K = \pi k/(N+1)$ and $k = 1, \dots, N$ is used as quantum label for this homogeneous case. These states are extended (delocalized) over the entire chain. It turns out that the state $k=1$ is the lowest (bottom) state of the exciton band. Close the bottom ($k \ll N$, i.e., $K \ll 1$) and in the limit of large N , the exciton dispersion relation reads³¹

$$E_k = -2.404 J + J \left(\frac{3}{2} - \ln K\right) K^2. \quad (3)$$

Furthermore, assuming that the chain is short compared to an optical wavelength, the oscillator strengths of the states $|k\rangle$ close to the bottom of the band are given by

$$F_k = \frac{2}{N+1} \left(\sum_{n=1}^N \sin Kn\right)^2 = \frac{1 - (-1)^k}{N+1} \frac{4}{K^2}, \quad (4)$$

where, the oscillator strength of a single molecule is set to unity. According to Eq. (4), the lowest state $k=1$ (with the energy $E_1 = -2.404J$) accumulates almost the entire oscillator strength, $F_1 = 0.81(N+1)$. Its radiative rate thus given is $\gamma_1 = \gamma_0 F_1 = 0.81 \gamma_0 (N+1)$, i.e., roughly N times larger than the radiative rate γ_0 of a monomer.³² The $k=1$ state is therefore referred to as the superradiant state. The oscillator strengths of the other odd states ($k=3, 5, \dots$) are much smaller, $F_k = F_1/k^2$, while the even states ($k=2, 4, \dots$) carry no oscillator strength at all, $F_k = 0$. As a consequence, the exciton absorption band occurs at the bottom of the exciton band, redshifted with respect to the monomer absorption band. This is characteristic for J aggregates.

In the presence of disorder ($\sigma \neq 0$), the exciton wave functions become localized on segments that are smaller than the chain length N . One of the important consequences of

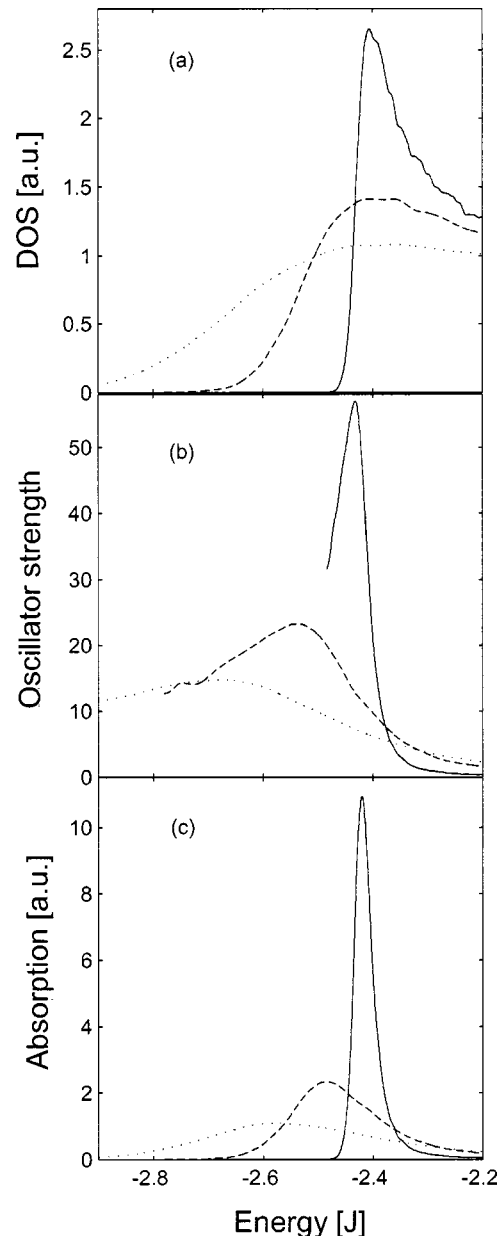


FIG. 1. (a) Density of states $\rho(E)$, (b) oscillator strength per state $F(E)$, and (c) absorption spectrum $A(E)$ calculated for different disorder strengths: $\sigma=0.1J$ (solid), $\sigma=0.3J$ (dashed), and $\sigma=0.5J$ (dotted). The disorder results in a tail of states below the bare exciton band edge $E_1 = -2.404J$, which is more pronounced for larger degree of disorder. Each spectrum for the oscillator strength per state has a well defined maximum and shows that the states in the tail carry most of the oscillator strength. This spectrum also tends to widen upon increasing σ/J . The absorption spectra simply reflect the fact that $A(E) = \rho(E)F(E)$.

this localization is the appearance of states below the bare exciton band bottom $E_1 = -2.404J$; these states form a tail of the density of states and in fact carry most of the oscillator strength. As a consequence, the linear absorption spectrum of the exciton system is spectrally located at this tail. All these properties are illustrated in Fig. 1, where the density of states, $\rho(E)$, the absorption spectrum, $A(E)$, and the oscillator strength per state, $F(E) = A(E)/\rho(E)$, are depicted for three values of the disorder strength: $\sigma=0.1J$, $0.3J$, and $0.5J$. These quantities have been calculated in the standard way using numerical simulations and the definitions

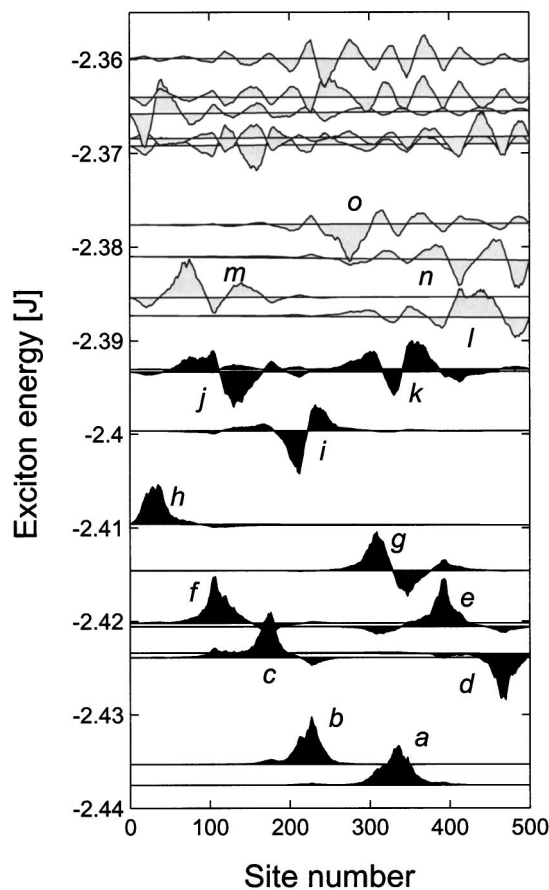


FIG. 2. Exciton wave functions φ_{vm} and energy levels E_v in the vicinity of the bottom of the exciton band for a particular realization of the disorder at $\sigma=0.1J$. The states are obtained by numerically diagonalizing the exciton Hamiltonian H_{nm} for a chain of 500 sites. The baseline of each state represents its energy in units of J . The wave function amplitudes are in arbitrary units. It is seen that the lower states (filled in black) are localized on segments of the chain with a typical size small compared to the chain length. Some of these localized states can be grouped into local manifolds of two or sometimes three states that overlap well with each other and overlap much weaker with the states of other manifolds [see the doublets of states (b,i) and (f,j) , and the triplet (a,g,k)]. The higher states (filled in gray) are more extended and cover several segments at which the lower states are localized.

$$\rho(E) = \frac{1}{N} \left\langle \sum_{v=1}^N \delta(E - E_v) \right\rangle, \quad (5a)$$

$$A(E) = \frac{1}{N} \left\langle \sum_{v=1}^N \left(\sum_{n=1}^N \varphi_{vn} \right)^2 \delta(E - E_v) \right\rangle, \quad (5b)$$

where the angular brackets denote the average over the disorder realizations. The statistics was improved using the smoothing technique developed in Ref. 33.

Despite the fact that the tail of the density of states does not show any spectral structure, it has been shown that the exciton wave functions and energy levels in this spectral region do exhibit a specific (local) structure.^{17,31,34–36} This structure is revealed by plotting the wave functions obtained for a particular realization of the disorder (see Fig. 2 for the case of $\sigma=0.1J$). The tail states (filled in black) have an appreciable amplitude only on localized segments of a typical size N^* (localization length; in the current example $N^* \approx 50$).

Some of them have no nodes within the localization segments (states $a-f$ and h in Fig. 2). Such states can be interpreted as local excitonic ground states. They carry large oscillator strengths, approximately N^* times larger than that of a monomer, and thus mainly contribute to the excitonic absorption and emission. The typical spontaneous emission rate of these states is $\gamma_1^* \approx \gamma_0 N^*$.

Some of the local ground states have partners localized on the same segment; examples are the doublets of states (b,i) and (f,j) in Fig. 2. These partner states have a well defined node within the localization segment and can be assigned to the first (local) excited state of the segment. Their oscillator strengths are typically several times smaller than those of the local ground states. Sometimes, but less frequently, a local manifold contains three states, such as the triplet (a,g,k) , with the third state being similar to the second excited state of the segment and having an oscillator strength small compared to that of the local ground state as well. The rest of the local ground states (see the states c, d, e , and h) do not have well defined partners, because the latter (higher in energy) are extended over a few (adjacent) N^* -site segments (the states l, m, n , and o). The oscillator strengths of these high-energy states are also small compared to those of the local ground states. Such states form mixed manifolds.

The mean energy spacing between the levels of a segment represents the natural energy scale in the tail of the density of states. The local spectral structure corresponding to this spacing, however, turns out to be hidden in the total density of states, because the mean absolute energy difference between the local ground states of different segments is approximately 1.5 times as large as the energy spacing between states within a single segment.³⁵ In spite of the fact that this local structure is not visible in the density of states and the absorption spectrum, it is clear that it plays a crucial role in the low-temperature dynamics of the excitons, because the dynamics is governed by the local structure of wave functions and spectral distribution.

As observed in Fig. 2, above the states that extend over a few adjacent segments, states occur that are extended over many segments; they hardly carry any oscillator strength at all. In spite of this, these states play an important role in the problem of the temperature dependence of the exciton fluorescence decay time. Increasing the temperature, leads to their thermal population, which in turn leads to slowing down the fluorescence decay.

To end this section, we stress that the segment size N^* has the meaning of a typical number and in practice undergoes large fluctuations.³⁵ First, the actual localization length of exciton states, as may for instance be assessed from the participation ratio, is energy dependent; it becomes smaller towards lower energy and even over the narrow region of the absorption band, this difference may be sizable.^{37,38} Second, even when we focus on a narrow region within the absorption band, the stochastic nature of the disordered system gives rise to large fluctuations in the localization size of the exciton wave functions. For the optical dynamics, it is important that these fluctuations are also reflected in fluctuations of the oscillator strength of the exciton states. To illustrate this, we plot in Fig. 3(a) the simulated distribution of

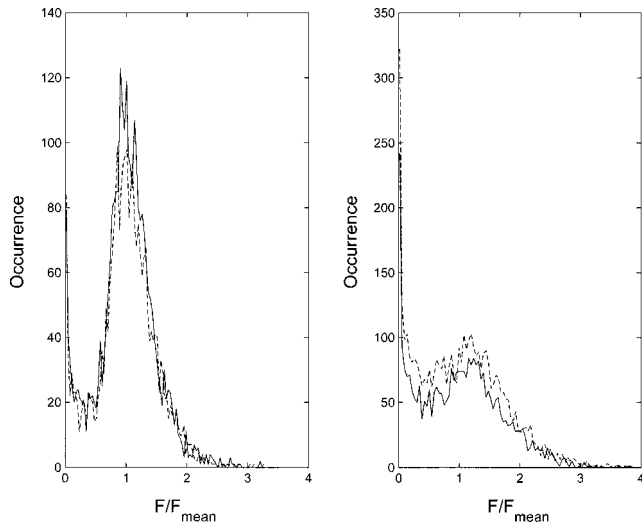


FIG. 3. Distributions showing the statistics of the dimensionless oscillator strength per state, $F_\nu = (\sum_{n=1}^N \varphi_{\nu n})^2$, collected in two narrow energy intervals of width $\delta E = 0.01J$. For the left panel this energy interval was chosen to be centered at the maximum of the spectrum of the oscillator strength per state [see Fig. 1(b)], while for the right panel this interval was centered at the maximum of the absorption band. In each panel, solid (dashed) lines correspond to $\sigma = 0.1J$ ($\sigma = 0.5J$). For each disorder strength, the distributions were collected using 5000 random realizations of the disorder on linear chains of $N = 500$ sites. To stress the invariant nature of the distributions, the oscillator strengths have been rescaled by the average value F_{mean} of F_ν in the interval and for the disorder strength under consideration. It is clearly seen that the width of each of the distributions is of the order of its mean.

the oscillator strength per state in an energy interval of width $\delta E = 0.01J$ centered at the energy where the average oscillator strength per state has its maximum [Fig. 1(b)]. In Fig. 3(b), this is repeated with the narrow interval centered at the energy where the absorption spectrum has its maximum [Fig. 1(c)]. The solid lines give the distributions for $\sigma = 0.1J$, while the dashed lines correspond to $\sigma = 0.5J$. The oscillator strength is given in units of its mean value F_{mean} within the energy interval under consideration and at the disorder value considered [for $\sigma = 0.1J$ ($0.5J$), $F_{\text{mean}} = 48$ (13) at the absorption peak and $F_{\text{mean}} = 57$ (15) at the peak of the oscillator strength per state]. We make the following observations: (i) the distributions have a width that is comparable to their mean, confirming the large fluctuations in segment size and extent and shape of the wave functions. (ii) In both narrow energy intervals, states are found with hardly any oscillator strength, which indicates that at both energies states occur with nodes. From the distributions it appears that such states with nodes are more abundant at the center of the absorption band (i.e., towards higher energy), which is consistent with the above explained local structure. We have confirmed this by doing a statistical analysis of the node structure of the wave function, using the value of $|\sum_n \varphi_{\nu n} \varphi_{\nu n}|$ (cf. the criterion for the node structure developed in Ref. 35). (iii) Interestingly, the distributions plotted on the scale of F_{mean} appear to be invariant under changing the disorder strength. This is consistent with an invariance of the local structure of the exciton energies and wave functions near the lower band edge.

III. INTRABAND RELAXATION MODEL

To describe the dynamics of the exciton eigenstates $|\nu\rangle$ of the Hamiltonian with site disorder, we will account for the effect of spontaneous emission and the scattering of excitons on lattice vibrations. We will describe this combined dynamics on the level of a Pauli master equation for the populations $P_\nu(t)$ of the exciton states

$$\dot{P}_\nu = -\gamma_\nu P_\nu + \sum_{\mu=1}^N (W_{\nu\mu} P_\mu - W_{\mu\nu} P_\nu), \quad (6)$$

where the dot denotes the time derivative, $\gamma_\nu = \gamma_0 (\sum_{n=1}^N \varphi_{\nu n})^2 = \gamma_0 F_\nu$ is the spontaneous emission rate of the exciton state $|\nu\rangle$ (with F_ν the dimensionless oscillator strength), and $W_{\nu\mu}$ is the transition rate from the localized exciton state $|\mu\rangle$ to the state $|\nu\rangle$. This transition rate is crucial in the description of the redistribution of the exciton population over the localized exciton states. The model for $W_{\nu\mu}$ is based on certain assumptions about the coupling between the excitons and the lattice vibrations. In Refs. 13 and 16, only the coupling between the excitons and the vibrations of the linear chain itself was taken into account. In reality, however, the exciton chains that we are interested in, such as linear aggregates, are not isolated, but are embedded in a host medium, so that the excitons are coupled to the host vibrations as well. The density of states of the latter is large compared to that of the vibrations of the chain itself. For this reason, it is natural to assume that it is the coupling of the excitons to the host vibrations that determines the exciton intraband relaxation in the linear chain.

In this article, we adopt the glassy model for $W_{\nu\mu}$ which we have introduced in our previous publication dealing with homogeneous molecular aggregates.¹⁹ This model assumes a weak linear on-site coupling of the excitons to acoustic phonons of the host medium and ignores correlations in the displacements of the different sites on the chain. Within this model, the transition rates are given by (see for details Ref. 19)

$$W_{\nu\mu} = W_0 S(E_\nu - E_\mu) \sum_{n=1}^N \varphi_{\nu n}^2 \varphi_{\mu n}^2 \times \begin{cases} n(E_\nu - E_\mu), & E_\nu > E_\mu, \\ 1 + n(E_\mu - E_\nu), & E_\nu < E_\mu. \end{cases}$$

Here, the constant W_0 is a parameter that characterizes the overall strength of the phonon-assisted exciton scattering rates. Its microscopic definition involves the nearest-neighbor excitation transfer interaction J , the velocity of sound in the host medium, and the mass of the sites in the exciton chain.¹⁹ In this article, we will consider W_0 as one composite parameter, which may be varied to account for different host and (or) exciton systems. The spectral factor $S(E_\nu - E_\mu)$ describes that part of the $|E_\nu - E_\mu|$ dependence of $W_{\nu\mu}$ which derives from the exciton-phonon coupling and the density of phonon states. The sum over sites in Eq. (7) represents the overlap integral of exciton probabilities for the states $|\mu\rangle$ and $|\nu\rangle$. Finally, $n(\Omega) = [\exp(\Omega/T) - 1]^{-1}$ is the mean occupation number of a phonon state with energy Ω (the Boltzmann constant is set to unity). Due to the presence

of the factors $n(\Omega)$ and $1+n(\Omega)$, the transition rates meet the principle of detailed balance: $W_{\nu\mu} = W_{\mu\nu} \exp[(E_\nu - E_\mu)/T]$. Thus, in the absence of radiative decay ($\gamma_\nu=0$), the eventual (equilibrium) exciton distribution is the Boltzmann distribution.

Within the Debye model for the density of phonon states, the spectral factor is given by¹⁹ $S(E_\nu - E_\mu) = (|E_\nu - E_\mu|/J)^3$. It is worth noting, however, that the applicability of this model to glassy host media is restricted to a very narrow frequency interval of the order of several wave numbers (see, for instance, Refs. 39 and 40). Therefore, we rather consider a simple linear approximation for this factor, $S(E_\nu - E_\mu) = |E_\nu - E_\mu|/J$, which is similar to the dependence used in Refs. 18 and 30. This scaling properly accounts for a decrease of the exciton-phonon interaction in the long-wave acoustic limit^{41,42} and prevents the divergence of $W_{\nu\mu}$ at small values of $|E_\nu - E_\mu|$. We checked that the results reported in this article are not essentially affected by assuming a higher power in the dependence of $W_{\nu\mu}$ on the energy mismatch.

In disordered systems, the overlap integral $\sum_{n=1}^N \varphi_{\nu n}^2 \varphi_{\mu n}^2$ appearing in the expression for $W_{\nu\mu}$ plays a much stronger role in the optical dynamics than the details of the dependence of S on the energy mismatch. The fact that $W_{\nu\mu}$ is proportional to this overlap integral allows one to distinguish between two types of exciton transitions occurring in the vicinity of the bottom of the exciton band (the region of main interest at low temperatures), namely intrasegment and intersegment transitions. These two types of transitions involve, respectively, states localized on the same localization segment of the chain and states localized on different segments. As has been established in Ref. 36, for both processes the overlap integrals scale inversely proportional to the typical segment size N^* , while numerically the intrasegment overlap integral is approximately 50 times as large as the intersegment one (independent of the disorder strength σ). Furthermore, the overlap integrals between the local states of a segment and one of the higher states that is extended over the same segment as well as the adjacent ones (such as the states l, m, n , and o in Fig. 2), are of the same order as the intrasegment overlap integral. This implies a specific scenario for the exciton intraband relaxation at low temperatures. Let us assume that the exciton, initially created in the blue tail of the absorption band (a condition which is usually met in experiments), quickly relaxes to one of the exciton states of a local manifold. Denote the two local states involved by the quantum labels 1 (ground state) and 2 (excited state). Because of the difference in intra- and intersegment overlap integrals discussed above, the exciton first relaxes within the local manifold, provided that the intrasegment transition rate is larger than the radiative rates γ_μ ($\mu=1, 2$). Only after this first step of relaxation, the exciton can hop to the states of other (adjacent) local manifolds, again, provided the intersegment hopping rate is larger than γ_μ . Note, that if γ_μ is larger than any transition rate $W_{\nu\mu}$, the exciton emits a photon before any relaxation step (intra- or intersegment) occurs. On this basis, one may distinguish between a fast and a slow limit of intrasegment relaxation. To this end, we compare the typical value of the intrasegment transition rate W_{12} at zero

temperature, with the radiative rate γ_1 of the local ground state. If $W_{12} > \gamma_1$, we are in the fast-relaxation limit. This inequality guarantees that at zero temperature, the exciton fluorescence decay is governed by the radiative process with a rate of the order of γ_1 . By contrast, if $W_{12} < \gamma_1$, the intrasegment relaxation rate W_{12} dictates the exciton fluorescence decay. This is very similar to the distinction of fast and slow relaxation which we have previously made in the case of fully delocalized excitons in homogeneous molecular aggregates.¹⁹ The reader may find an elaborate discussion on the principle difference between these two limits in Ref. 19.

For the remainder of this article, it is useful to find the value of W_0 that distinguishes between the limits of fast and slow intrasegment relaxation; we will denote this value by W_0^{intra} . Thus, the inequalities $W_0 \gg W_0^{\text{intra}}$ and $W_0 \ll W_0^{\text{intra}}$ determine the fast and slow regimes of intrasegment relaxation, respectively. We first estimate W_{12} by replacing $\sum_n \varphi_{\nu n}^2 \varphi_{\mu n}^2$ by $1/N^*$, giving $W_{12} = W_0(E_2 - E_1)/JN^*$. Then we equate W_{12} to the superradiant decay rate γ_1 , which is typically $\gamma_0 N^*$, and obtain

$$W_0^{\text{intra}} = \frac{\gamma_0 J N^{*2}}{E_2 - E_1}. \quad (7)$$

If we restrict for a moment to nearest-neighbor interactions, we may even go one step further by realizing that, as a consequence of wave vector quantization and level repulsion within localization segments, the typical energy difference $E_2 - E_1$ then scales like $E_2 - E_1 \approx 3\pi^2 J/N^{*2}$,^{17,35,43} which leads to

$$W_0^{\text{intra}} = (3\pi^2)^{-1} \gamma_0 N^{*4}. \quad (8)$$

From this expression, it is clear that W_0^{intra} steeply decreases with decreasing segment size, i.e., with increasing degree of disorder. This steep scaling is not essentially affected by taking into account long-range dipole-dipole interactions. Thus, if the degree of disorder increases and the excitons become more localized, there is a strong tendency of the system to move into the fast-relaxation limit, where the radiative decay governs the fluorescence kinetics.

Following intraband relaxation, the next relaxation step involves transitions between states of different segments (exciton migration). Similarly to the above, one may distinguish the limits of fast and slow intersegment relaxation, defined as $W_{1,1'} > \gamma_1$ and $W_{1,1'} < \gamma_1$, respectively. Here, the states 1 and 1' denote the ground states localized on adjacent segments and it is assumed that $E_1 > E_{1'}$. If the transfer process is slow, the exciton spontaneously decays before it makes a hop to an adjacent localization segment with $E_{1'} < E_1$. As a result, the fluorescence spectrum is expected to coincide with the absorption band, because the latter is mainly determined by the total collection of local ground states (the segment states with appreciable oscillator strength), i.e., in the absorption spectrum each local ground state contributes, independent of the value of its energy. However, if the intersegment transfer process is fast, the exciton can make downhill hops before the fluorescence is emitted. Therefore, lower-energy local ground states will give a larger contribution to the fluorescence spectrum than higher-energy ones; this gives rise to a visible redshift (Stokes shift) of the fluorescence

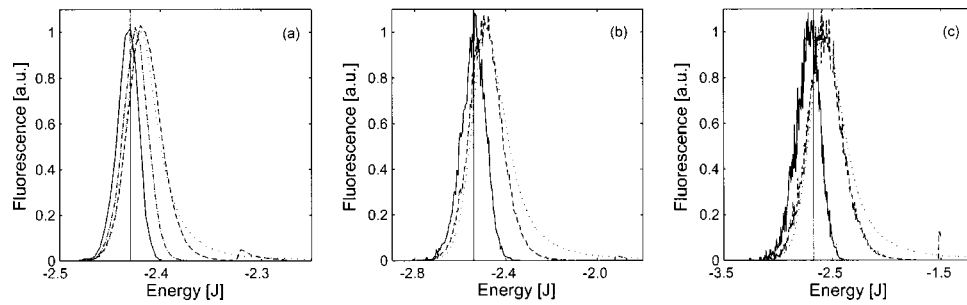


FIG. 4. Zero-temperature steady-state exciton fluorescence spectra calculated for various disorder strengths σ and exciton scattering rates W_0 . Spectra were obtained by numerical solution of the steady-state master equation Eq. (10) under the condition of off-resonance blue-tail optical pumping: (a) $\sigma=0.1J$, with $W_0=J$ (dashed), $W_0=100J$ (dashed-dotted), and $W_0=10^2J$ (solid); (b) $\sigma=0.3J$, with $W_0=0.1J$ (dashed) and $W_0=100J$ (solid); (c) $\sigma=0.5J$, with $W_0=0.01J$ (dashed) and $W_0=100J$ (solid). The dotted line in each panel represents the absorption band, while the solid vertical line shows the location of the maximum of the spectrum for the oscillator strength per state. The other parameters used in the simulations were $N=500$, $J=600\text{ cm}^{-1}$, and $\gamma_0=2 \times 10^{-5} J$. The average was performed over 5000 realizations of the disorder, using energy bins of $0.005J$ to collect the fluorescence spectrum.

spectrum with respect to the absorption band (see Sec. IV B). Using the above noted factor of 50 difference between the intra- and intersegment overlap integrals,³⁶ the value of W_0 that distinguishes between the limits of fast and slow intersegment relaxation, denoted by W_0^{inter} , is given by $W_0^{\text{inter}} = 50W_0^{\text{intra}}$. With reference to Eq. (8), we note that, keeping W_0 constant, a Stokes shift is expected to become more noticeable for smaller segments, i.e., for growing disorder strength.

IV. STEADY-STATE FLUORESCENCE SPECTRUM

In this section, we deal with the exciton dynamics and the corresponding fluorescence spectrum under steady-state conditions, which are maintained by optically pumping the system. The steady-state fluorescence spectrum is defined as

$$I(E) = \frac{1}{N} \left\langle \sum_{\nu} \delta(E - E_{\nu}) \gamma_{\nu} P_{\nu}^{\text{st}} \right\rangle, \quad (9)$$

where P_{ν}^{st} is the solution of the steady-state master equation

$$0 = R_{\nu} - \gamma_{\nu} P_{\nu}^{\text{st}} + \sum_{\mu=1}^N (W_{\nu\mu} P_{\mu}^{\text{st}} - W_{\mu\nu} P_{\nu}^{\text{st}}), \quad (10)$$

where R_{ν} denotes the constant rate of optically creating population in the ν th exciton state by a cw pump pulse.

We performed numerical simulations of exciton fluorescence spectra, by solving the master equation Eq. (10) for randomly generated realizations of the disorder. For each realization, we diagonalize the Hamiltonian H_{nm} in order to calculate the radiative constants γ_{ν} and the transition rates $W_{\nu\mu}$ entering the master equation. In all simulations reported in the remainder of this article, we set $J=600\text{ cm}^{-1}$ ($1.8 \times 10^{13}\text{ s}^{-1}$) and $\gamma_0=2 \times 10^{-5} J$ ($3.6 \times 10^8\text{ s}^{-1}$). These parameters are quite typical for molecular aggregates of poly-methine dyes, such as PIC.

A. Steady-state fluorescence spectra at zero temperature

In this section, we concentrate on the zero-temperature fluorescence spectra, which may be used to illustrate the different regimes of exciton relaxation. In Fig. 4 we present by dashed and solid lines the zero-temperature steady-state fluo-

rescence spectra for various combinations of values of the disorder strength σ and the phonon-assisted exciton scattering strength W_0 . All spectra were calculated under the condition of off-resonance optical pumping in a narrow energy window of width $0.05J$ in the blue tail of the absorption band. The exact position of the pump window was chosen to be blueshifted relative to the maximum of the absorption band (simulated at the same value of the disorder strength) by three times the full width at half maximum (FWHM) of this band. The pump rate of each exciton state ν inside the pump window was taken proportional to its oscillator strength: $R_{\nu}=F_{\nu}$. As clear from Fig. 4, for each value of σ , the fluorescence spectrum nearly follows the absorption band (shown by the dotted line) as long as W_0 is small, while this spectrum experiences a visible Stokes shift if W_0 is increased. This agrees with our expectations formulated in Sec. III. Also in agreement with our arguments made at the very end of Sec. III, we observe that (for constant W_0) the magnitude of the Stokes shift is smaller for smaller disorder strength.

To gain more quantitative insight into the above behavior of the fluorescence spectra, let us estimate the values of the parameters W_0^{intra} and W_0^{inter} that distinguish the limits of fast and slow relaxation for intra- and intersegment transitions, respectively, as introduced in Sec. III. First, we do this for the largest disorder strength considered in the simulations, $\sigma=0.5J$ [Fig. 4(c)]. From the maximum of the spectrum for the oscillator strength per state plotted in Fig. 1(b), we find as typical segment size $N^*=15$ for this disorder strength. Similarly, the typical separation between the two bottom states of a localization segment may be estimated from the FWHM of the absorption band, giving $E_2-E_1=0.4J$ [Fig. 1(c)]. Substituting these data into Eq. (7), we obtain $W_0^{\text{intra}} \approx 0.01J$ and $W_0^{\text{inter}} = 50W_0^{\text{intra}} \approx 0.5J$. Thus, the smaller value of W_0 considered in the simulations ($0.01J$) is equal to W_0^{intra} , while it is much smaller than W_0^{inter} , i.e., no intersegment hops will occur prior to fluorescent emission. The latter explains why there is no Stokes shift of the fluorescence spectrum. On the other hand, as the system is in the intermediate regime with regards to the intrasegment hopping ($W_0=W_0^{\text{intra}}$), the radiative channel can compete with the intrasegment relaxation. This explains the presence of the

small and narrow fluorescence peak coinciding with the pumping interval in the blue tail of the absorption spectrum. By contrast, the higher value of $W_0=100J$ exceeds $W_0^{\text{inter}}=0.5J$ by more than two orders of magnitude. This results in a visible Stokes shift of the fluorescence spectrum as well as a strong reduction of the fluorescence in the excitation window.

Analogous estimates performed for $\sigma=0.1J$ [Fig. 4(a)] bring us to the following results: $W_0^{\text{intra}}\approx J$ and $W_0^{\text{inter}}=50W_0^{\text{intra}}\approx 50J$. Here we used $N^*=57$ and $E_2-E_1=0.04J$, taken as previously from Figs. 1(b) and 1(c), respectively. For the smaller value of $W_0=J$, the excitons are again within the intermediate regime with regards to the intrasegment relaxation. As a consequence, the fluorescence spectrum shows the same peculiarities as in the case of $\sigma=0.5J$ at $W_0=0.01J$. However, as the higher value of $W_0=100J$ is only twice as large as compared to $W_0^{\text{inter}}\approx 50J$, the Stokes shift here is smaller than in the case of the higher disorder magnitude. A large Stokes shift may be forced by taking $W_0=10^5J$, as is also illustrated in Fig. 4(a). It should be noted, however, that this large value for W_0 lies outside the range of validity of our theory. The reason is that such a large scattering rate leads to $W_{12}\gg E_2-E_1$ ($W_{12}\approx 0.8J$ for the current example), which implies that the second-order treatment of the exciton-phonon interaction is a poor approximation. More importantly, under such conditions the segment picture breaks down, because the exciton coherence size is dominated by the scattering on phonons instead of static disorder. A proper description then requires using a density matrix approach.^{44,45}

B. Temperature dependence of the Stokes shift

We now turn to the temperature dependence of the steady-state fluorescence spectrum. In particular, we are interested in the temperature dependence of its Stokes shift with respect to the absorption band. We have calculated this shift as the difference in peak positions between the absorption and fluorescence bands. As the simulated fluorescence spectrum contains appreciable stochastic noise (it is not possible to apply the same smoothing as may be used when simulating the absorption spectrum³³), its peak position was determined by fitting the upper half of the peak to a Gaussian line shape. Figure 5 shows the obtained results, for three different values of W_0 at a fixed disorder strength, $\sigma=0.3J$. The characteristic peculiarity of all curves is that they are nonmonotonic: the Stokes shift first increases upon heating and then goes down again. The extent of the temperature interval over which the Stokes shift increases is small compared to the absorption band width, which is 170 K for the current degree of disorder. A Stokes shift that increases with temperature is counterintuitive, because, at first glance, it seems that the temperature should force the excitons to go up in energy, giving rise to a monotonic decrease of the Stokes shift. This expected behavior is indeed observed in inhomogeneously broadened systems doped with point centers like, for instance, glasses doped with rare-earth ions.⁴⁶ The explanation for the peculiar behavior of the Stokes shift in the Frenkel exciton chain is similar to that for the nonmonotonic

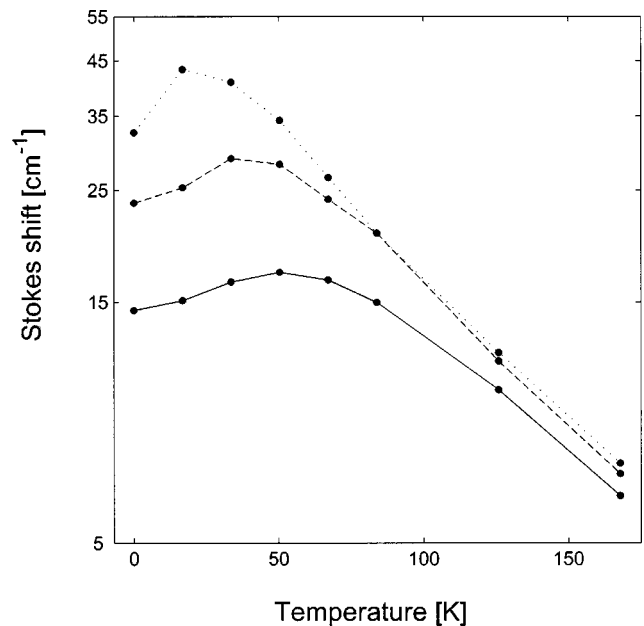


FIG. 5. Semilog plots of the temperature dependence of the Stokes shift of the fluorescence spectrum at the disorder strength $\sigma=0.3J$, for different exciton scattering rates: $W_0=J$ (solid), $W_0=10J$ (dashed), and $W_0=100J$ (dotted). The data were obtained by numerical solution of the master equation Eq. (10) under the condition of off-resonance blue-tail excitation. The dots mark the numerical data, while the lines connecting the dots are guides to the eye. The other parameters used in the simulations were $N=500$, $J=600\text{ cm}^{-1}$, and $\gamma_0=2\times 10^{-5}J$. The average was performed over 5000 realizations of the disorder.

behavior found for disordered quantum wells,²⁴ and resides in a thermally activated escape from local potential minima. However, for the case of the disordered linear chain, the detailed knowledge of the low-energy spectral structure provides additional means to unravel the characteristics of this behavior.

Let us first recall the zero-temperature scenario of the exciton relaxation. Excitons created initially at the blue tail, rapidly relax to the local states of the DOS tail, which are visible in fluorescence. After that, the excitons may relax further, within the manifold of the local ground states. At zero temperature, however, this possibility is very restricted. The reason is that an exciton that relaxed into one of the local ground states may move to another similar state of an adjacent localization segment only when the latter has an energy lower than the former and W_0 exceeds W_0^{inter} (Sec. III). The typical energy difference between the local ground states is of the order of the absorption band width. Therefore, after one jump the exciton typically resides in the red tail of this band. The number of states with still lower energy then strongly reduces, giving rise to an increased expectation value for the distance to such lower energy states. In fact, after one jump the exciton has a strongly suppressed chance to jump further during its lifetime; it will generally emit a photon without further jumps (migration). Thus, the states deep in the tail of the DOS can typically not be reached by the excitons, simply because they occur at a low density. This qualitatively explains why the Stokes shift of the fluorescence spectrum does not exceed the absorption band width, even for W_0 large compared to W_0^{inter} (see Fig. 4).

Upon a small increase of the temperature from zero, however, it becomes easier to reach those lower-lying states, because the spatial migration to other segments may take place by thermally activated transitions involving exciton states that are extended over several localization segments as intermediate states.⁴⁷ It is this indirect hopping that is responsible for the increase of the Stokes shift at temperatures small compared to the absorption band width. Further heating will thermalize the excitons and lead to real populations of higher-energy states; the Stokes shift will then decrease again.

To be more specific, we present estimates. We first note that the overlap integral of the squared wave functions in Eq. (7) for a local ground state 1 and a higher state 3 that extends over more than one segment, but still overlaps with the ground state 1, has the same order of magnitude as for the states 1 and 2 of a local manifold, i.e., $1/N^*$ then, the transition rate up from the ground state to the more extended state, W_{31} , can be estimated as $W_{31} \approx [W_0(E_3 - E_1)/JN^*] \exp[-(E_3 - E_1)/T]$. In order for the exciton migration via the higher state to be activated, W_{31} should be larger than $\gamma_1 = \gamma_0 N^*$, the spontaneous emission rate of state 1. Equating these two rates gives us a temperature T_0 at which the Stokes shift is increased over its zero-temperature value:

$$T_0 = (E_3 - E_1) / \ln \left[\frac{W_0(E_3 - E_1)}{\gamma_0 N^{*2} J} \right]. \quad (11)$$

Taking as an estimate for $E_3 - E_1$ the FWHM of the absorption band, $0.2J$ at $\sigma = 0.3J$, we obtain $T_0 = 57, 32$, and 22 K for $W_0 = J, 10J$, and $100J$, respectively. These numbers are in good agreement with the positions of the maxima of the curves in Fig. 5.

To the best of our knowledge, the only one-dimensional exciton system for which the temperature dependence of the Stokes shift has been measured, is the molecular aggregate that is formed by the cyanine dye THIATS.¹⁵ For this aggregate, a nonmonotonic temperature dependence of the Stokes shift was reported at low temperatures, very similar to our numerical results. Thus, the model we are dealing with provides an explanation of the behavior reported in Ref. 15. A detailed fit to these experimental data, also including the absorption spectrum and the fluorescence lifetime of this aggregate, will be presented in another article.⁴⁸

V. FLUORESCENCE DECAY TIME

We proceed to study the decay time of the total time-dependent fluorescence intensity following pulsed excitation at $t = 0$. This intensity reads

$$I(t) = \left\langle \sum_{\nu} \gamma_{\nu} P_{\nu}(t) \right\rangle, \quad (12)$$

where the $P_{\nu}(t)$ are obtained from the Pauli master equation Eq. (6) with the appropriate initial conditions. The proper definition of the decay time requires attention, as the time dependence of $I(t)$ is not monoexponential. We already encountered this problem for homogeneous aggregates,¹⁹ but for the disordered systems under consideration, the problem

is even more obvious. The multiexponential behavior is a consequence of the large fluctuations in the spontaneous decay rates of different exciton states, as is clearly demonstrated by the distribution of exciton oscillator strengths plotted in Fig. 3. Similarly, large fluctuations occur in the transition rates $W_{\nu\mu}$. The simplest solution is to define the decay time, τ_e , as the time it takes the fluorescence intensity $I(t)$ to decay to $1/e$ of its peak value $I(t_{\text{peak}})$:

$$I(t_{\text{peak}} + \tau_e) = \frac{1}{e} I(t_{\text{peak}}). \quad (13)$$

Throughout this article, we will use this definition of the decay time. It should be noted that in the case of initial excitation in the blue tail of the absorption band, $t_{\text{peak}} \neq 0$, due to the fact that a finite time elapses before the exciton population reaches the lower-lying emitting states. An alternative choice for the decay time is the expectation value of the photon emission time, $\tau = \int_0^{\infty} \langle \sum_{\nu} P_{\nu}(t) \rangle dt$. For monoexponential decay, both definitions give the same result, but in general this does not hold. In particular, for nonexponential fluorescence kinetics, the latter definition, τ , only gives a meaningful measure of the fluorescence time scale in the limit of the fast intrasegment relaxation (for more details see Ref. 19).

A. Broadband resonance excitation

We first consider the case of broadband resonance excitation, which is similar to what takes place in echo experiments.⁴⁹ Under this condition, all states are excited with a probability that is proportional to their respective oscillator strengths, $P_{\nu}(t=0) = F_{\nu}$, meaning that the spectral profile of the initially excited states coincides with the absorption band. Thus, the initial exciton population mostly resides in the superradiant states.

In Figs. 6(a)–6(c), we depicted the temperature dependence of the fluorescence decay time τ_e for three different disorder strengths, $\sigma = 0.1J, 0.3J$, and $0.5J$, respectively; for each σ value two different strengths of the exciton scattering strength W_0 were considered. The solid line in each panel presents results for the intermediate regime with regards to the intrasegment relaxation, i.e., when $W_{21} \sim \gamma_1$, while the dashed line shows results in the limit of fast relaxation, $W_{21} \gg \gamma_1$. For all three disorder strengths, the higher value of W_0 considered, is below the threshold W_0^{inter} for fast intersegment relaxation, in other words, no visible Stokes shift occurs in the fluorescence spectra for any of the chosen parameters. Figure 6(a) shows on a semilog scale the time dependence of the fluorescent traces underlying the reported decay times for $W_0 = 10J$. These traces clearly show that in general the intensity decay is nonexponential.

It is worthwhile to estimate the zero-temperature values of the fluorescence decay time using the relationship $\tau_e = 1/(\gamma_0 N^*)$. For N^* we take the maximum value of the spectrum for the oscillator strength per state [Fig. 1(b)], i.e., $N^* = 57, 23$, and 15 for $\sigma = 0.1J, 0.3J$, and $0.5J$, respectively. Then, for the parameters used in our simulations, $\gamma_0 = 2 \times 10^{-5} J$ and $J = 600 \text{ cm}^{-1}$, the corresponding values of τ_e are $49, 121$, and 185 ps, respectively. These estimated times are larger than the calculated ones in Fig. 6. The reason for

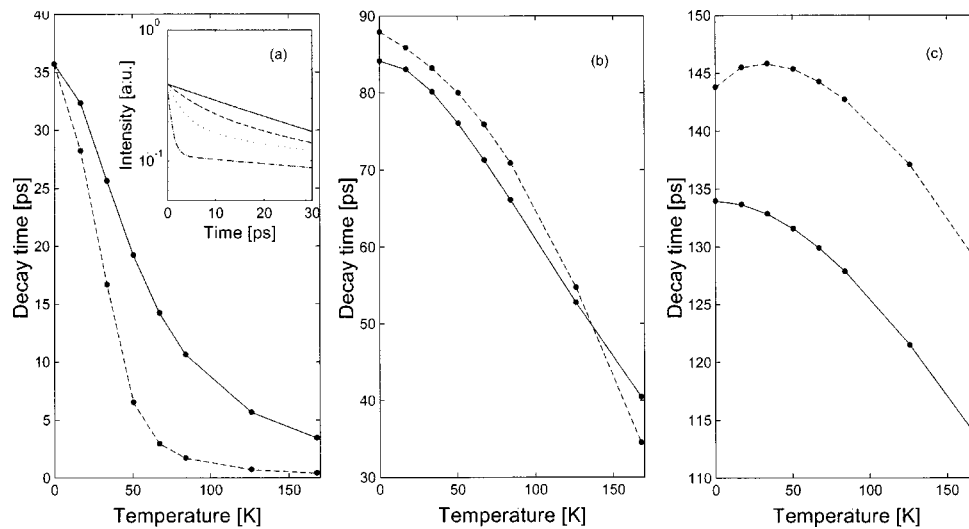


FIG. 6. Temperature dependence of the fluorescence decay time τ_e calculated for various disorder strengths σ and exciton scattering rates W_0 . The data were obtained by numerical solution of the master equation Eq. (6) under the condition of broadband resonant excitation, setting $P_\nu(t=0) = F_\nu$. The dots mark the numerical data, while the lines connecting the dots are guides to the eye: (a) $\sigma=0.1J$, with $W_0=J$ (solid) and $W_0=10J$ (dashed); (b) $\sigma=0.3J$, with $W_0=0.1J$ (solid) and $W_0=J$ (dashed); (c) $\sigma=0.5J$, with $W_0=0.01J$ (solid) and $W_0=J$ (dashed). The other parameters used in the simulations were $N=500$, $J=600 \text{ cm}^{-1}$, and $\gamma_0=2 \times 10^{-5} J$. The average was performed over 50 realizations of the disorder. The inset in (a) shows the time dependence of the fluorescence intensity for $W_0=10J$ at four different temperatures: from top to bottom, the curves correspond to $T=0, 17, 34$, and 84 K , respectively.

this deviation is the resonance excitation condition, combined with the large fluctuations in the oscillator strength per state (Fig. 3). The states with a higher than typical oscillator strength are excited to a larger extent than those with typical (and smaller) oscillator strengths. Obtaining a relatively large part of the initial population, they mainly determine the initial stage of the fluorescence kinetics. This gives rise to a faster decay rate than the typical one.

Apart from some low-temperature peculiarities of τ_e for higher degree of disorder, all curves in Fig. 6 tend to go down upon increasing the temperature. This has the following explanation. The uphill transition processes, which are characterized by the rate $W_{21} \propto \exp[-(E_2 - E_1)/T]$, come into play when the temperature is increased. At some disorder dependent temperature, W_{21} becomes larger than γ_1 , and the exciton population from the initially populated superradiant states is transferred to higher (dark, initially not excited) states. This nonradiative loss of population from the superradiant states gives rise to a drop in the fluorescence intensity, which contributes to the observed fluorescence decay. We stress that it is the rate W_{21} that determines the time of this uphill process (Ref. 19). Thus, with increasing temperature, the drop in the fluorescence decay time τ_e reflects in fact the shortening of the intrasegment relaxation time and not the exciton radiative lifetime.

To conclude this subsection, we note that the range of variation of the fluorescence decay time with temperature differs dramatically for different disorder strengths. In particular, for $\sigma=0.1J$, τ_e decreases from its maximal value of 36 ps (at $T=0$) to about 1 ps at 150 K, while for $\sigma=0.5J$ this drop consists of only 15%–20% of the zero-temperature value of τ_e . This simply results from the fact that the absorption band widths for these two values of the disorder strength are (in temperature units) 40 and 300 K, respectively. We recall that the rate of uphill transfer

$W_{21} \propto \exp[-(E_2 - E_1)/T]$, $E_2 - E_1$ being of the order of the absorption bandwidth. Thus, for $\sigma=0.1J$, a temperature of 40 K is already sufficient to activate the uphill transfer of population and to noticeably drop the fluorescence intensity. By contrast, even the highest temperature considered in the simulations, $T=160 \text{ K}$, is not enough to start the uphill process for $\sigma=0.5J$.

B. Off-resonance blue-tail excitation

We now turn to the case of off-resonance excitation in the blue tail of the absorption band. This is the usual situation in fluorescence experiments.^{5,7,8,10–12,14} We recall that in this case between the absorption and emission events an additional step exists: the vibration-assisted relaxation from the initially excited states to the radiating ones. This results in different scenarios for the exciton fluorescence kinetics, dependent on the relationship between the intraband relaxation rate and the rate of exciton spontaneous emission.¹⁹

In Fig. 7, we depict the temperature dependence of the fluorescence decay time τ_e obtained from numerical simulations for various strengths of the disorder σ and the vibration-assisted exciton scattering rate W_0 . The initial condition for solving Eq. (6) was taken $P_\nu(t=0) = F_\nu$ in a narrow window in the blue tail of the absorption band, defined in the same way as in Sec. IV A. The scattering rates W_0 were chosen to realize different limits of the intraband relaxation. In particular, in the case of the smallest disorder strength, $\sigma=0.1J$, the scattering rates $W_0=0.1J$ and $W_0=J$ describe the limits of intermediate and fast intrasegment relaxation, respectively (see Sec. IV A). However, with respect to the intersegment hopping, these values both correspond to the slow limit. Finally, the highest value of $W_0=100J$ describes the limit of fast intersegment relaxation. Similar re-

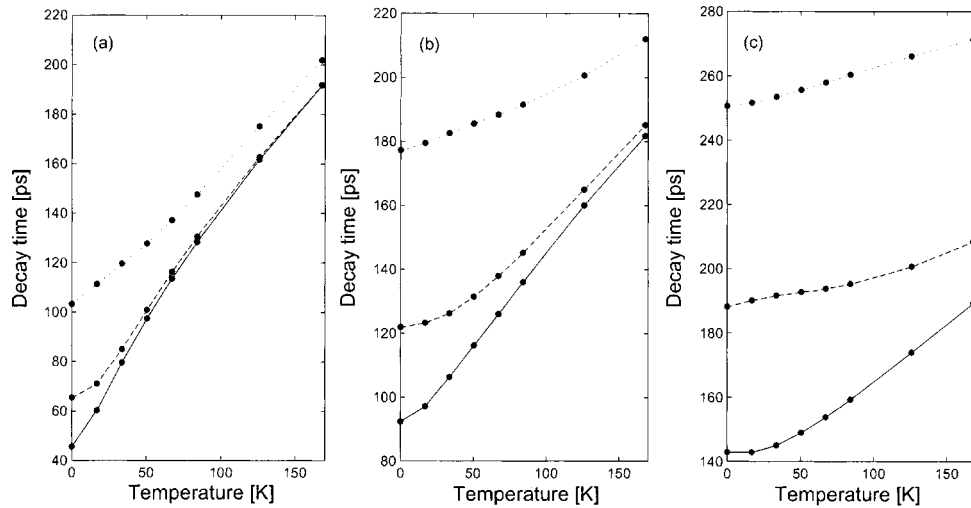


FIG. 7. Temperature dependence of the fluorescence decay time τ_e calculated for various disorder strengths σ and exciton scattering rates W_0 . The data were obtained by numerical solution of Eq. (6) under the condition of off-resonance blue-tail excitation. The dots mark the numerical data, while the lines connecting the dots are guides to the eye: (a) $\sigma=0.1J$, with $W_0=J$ (dotted), $W_0=10J$ (dashed), and $W_0=100J$ (solid); (b) $\sigma=0.3J$, with $W_0=0.1J$ (dotted), $W_0=J$ (dashed), and $W_0=10J$ (solid); (c) $\sigma=0.5J$, with $W_0=0.01J$ (dotted), $W_0=0.1J$ (dashed), and $W_0=J$ (solid). The other parameters used in the simulations were $N=500$, $J=600\text{ cm}^{-1}$, and $\gamma_0=2\times 10^{-5}J$. The average was performed over 50 realizations of the disorder.

relationships exist between the W_0 values for the other degrees of disorder.

Figure 7 shows that, in contrast to the case of the broadband resonance excitation, all τ_e curves go up almost linearly with temperature, independent of the values for σ and W_0 . Being well separated at zero temperature, they tend to approach each other at higher temperatures. The latter effect is more pronounced for smaller degrees of disorder. Some of the curves show a low-temperature plateau, whose extent is smaller than the absorption bandwidth. On the other hand, there is also a common feature between the resonant and off-resonant type of excitation: the range of variation of τ_e with temperature is smaller for more disordered systems. This effect has the same explanation as discussed in Sec. V A.

Two processes are responsible for the observed increase of τ_e with temperature: intraband downhill relaxation after the excitation event and thermalization of the excitons over the band. Let us consider the first step of the population transfer from the initially excited states to lower states, both dark and superradiant. An important feature of this process is that it is almost nonselective due to the linear dependence of the transition rates $W_{\nu\mu}$ on the energy mismatch. As a result, the lower states are populated almost equally, whether superradiant or dark. This is in sharp contrast to the case of resonance excitation where, in fact, only the superradiant states are initially excited. The further scenario can be understood by considering a simple two-level model. Let level 1 denote the lowest, superradiant, state of the local manifold, having an emission rate γ_1 , while level 2 is the higher-energy, dark, local state. We assume that following the fast initial relaxation described above, both levels are excited equally. The Pauli master equation Eq. (6) now reduces to

$$\dot{P}_1 = -(\gamma_1 + W_{21})P_1 + W_{12}P_2, \tag{14a}$$

$$\dot{P}_2 = -W_{12}P_2 + W_{21}P_1, \tag{14b}$$

with initial conditions $P_1(0)=P_2(0)=1/2$. We seek the solution of Eqs. (14) in the limits $W_{12}=W_{21}=W(T\gg E_2 - E_1)$ and $W\gg\gamma_1$ (fast intrasegment relaxation). It is easy to find that the intensity $I = -\dot{P}_1 = -\dot{P}_2 = \gamma_1 P_1$ is given by

$$I(t) = \gamma_1 \left(1 - \frac{\gamma_1}{4W} \right) e^{-\gamma_1/2t} + \gamma_1 \frac{\gamma_1}{4W} e^{-2Wt}. \tag{15}$$

The second term in Eq. (15) can be neglected. From the first one it follows that the fluorescence decay rate is given by $\gamma_1/2$, which directly reflects the exciton's radiative decay. It is only half the superradiant rate γ_1 due to the fast exchange of population between the superradiant level 1 and the dark level 2. If the temperature is increased, one should generalize this discussion by considering the situation where l nonradiating levels, equally populated initially, are rapidly exchanging population with the superradiant level. The number l increases with temperature. The result is straightforward: one should replace the rate $\gamma_1/2$ by $\gamma_1/(l+1)$. This qualitatively explains the temperature behavior of the exciton fluorescence decay time found in the simulations.

To conclude the discussion of the numerical results presented in Fig. 7, we comment on the zero-temperature value of τ_e . For each σ value, this noticeably depends on W_0 , decreasing as W_0 goes up. Furthermore, the calculated zero-temperature values for τ_e at the smallest magnitudes of W_0 considered in the simulations ($W_0=J$, $0.1J$, and $0.01J$ for $\sigma=0.1J$, $0.3J$, and $0.5J$, respectively), are larger than those estimated from the maximum of the spectrum for the oscillator strength per state [Fig. 1(b)]. Recall that these estimates are 49 ps for $\sigma=0.1J$, 121 ps for $\sigma=0.3J$, and 185 ps for $\sigma=0.5J$ (see Sec. V A).

The observed decrease of the zero-temperature value of τ_e with W_0 , may be understood from the fact that the emitting exciton sees a distribution of the oscillator strength that differs for different W_0 values. Below, we provide a qualitative picture of this. The exciton is initially excited at the blue

tail of the absorption band, where the oscillator strengths are small, so that downhill relaxation dominates over the emission. This allows the exciton to go down in energy until the intraband relaxation rate becomes comparable to or smaller than the radiative rate. Once this has happened the exciton emits a photon. Let us analyze first what happens at the smallest magnitudes of the exciton scattering rate W_0 considered in the simulations (see above). These values correspond to the intermediate case with regards to intrasegment relaxation, while with respect to the intersegment hopping, they fall in the slow limit. This means that the exciton, after it has relaxed from the blue-tail states to the superradiant states, does not move any more. It can then only emit a photon. The zero-temperature steady-state spectra presented in Fig. 4 provide information about the spectral location of the exciton emission. For the values of W_0 we are discussing, the emission spectra coincide in general with the absorption spectra. At the same time, the maximum of the oscillator strength distribution is shifted to the red from the absorption maximum (Fig. 1). Therefore, the fluorescence decay time is expected to be larger than that estimated via the maximum of the oscillator strength distribution. This explains the results of the simulations.

For the largest value of W_0 considered in the simulations ($W_0=100J$, $10J$, and J for $\sigma=0.1J$, $0.3J$, and $0.5J$, respectively), the limit of fast intersegment relaxation applies. This means that after the fast intrasegment relaxation to the superradiant states, the exciton still has a chance to relax further due to intersegment hops (migration). As a result, the emission spectra are shifted towards the maxima of the spectra of the oscillator strength per state (see Fig. 4), which explains the shortening of the decay time observed in the numerical simulations with increasing value of W_0 .

C. Dependence on the detection energy

To end our analysis of the fluorescence decay time, we address its dependence on the detection energy. This has attracted considerable attention in the literature on aggregates and polymers (see, for instance, Refs. 15 and 23). To study this dependence, we have simulated the detection dependent fluorescence intensity, defined through

$$I(E_d; t) = \left\langle \sum_{\nu} \gamma_{\nu} P_{\nu}(t) \Delta(E_d - E_{\nu}) \right\rangle, \quad (16)$$

where E_d denotes the central detection energy and $\Delta(E_d - E_{\nu})$ is the detection window, which is unity for $|E_d - E_{\nu}| < 0.0025J$ and zero otherwise. Simulations were carried out for aggregates of $N=250$ molecules with $\sigma=0.3J$ and $W_0=100J$, other parameters as usual. We have considered blue-tail short-pulse excitation conditions, as was done in Sec. VB, and three detection energies: the peak of the steady-state fluorescence spectrum [Fig. 4(b)], and the positions of the blue and red half maximums of this spectrum. From the intensity traces, we have extracted the energy dependent $1/e$ decay times $\tau_e(E_d)$. The results as a function of temperature are shown in Fig. 8, with the upper, middle, and lower curve corresponding to red, peak, and blue detection energy, respectively.

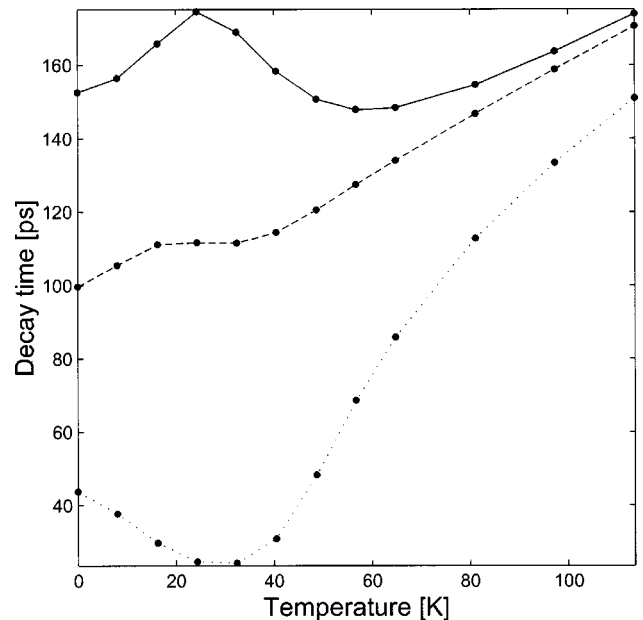


FIG. 8. Temperature dependence of the fluorescence decay time $\tau_e(E_d)$ calculated for aggregates of $N=250$ molecules, with $J=600 \text{ cm}^{-1}$, $\gamma_0=2 \times 10^{-3}J$, $\sigma=0.3J$, and $W_0=100J$. The data were obtained by numerical solution of Eq. (6) under the condition of off-resonance blue-tail excitation. The dots mark the numerical data, while the lines connecting the dots are guides to the eye. The three curves correspond to different detection energies E_d related to the steady-state fluorescence spectrum in Fig. 4(b): detection at the position of the red half maximum of this spectrum (solid line), at the peak of this spectrum (dashed line), and at the blue half maximum (dotted line). The average was performed over 10 000 realizations of the disorder.

We see that at zero temperature the decay times clearly differ for the three detection energies. For the case of red detection, we observe a decay time of 152 ps. Based on the average oscillator strength per state at this red-wing energy, we arrive at a purely radiative decay time $[1/\gamma_0 F(E)]$ of 145 ps. The agreement between these numbers indicates that at the red side the decay time at zero temperature is determined completely by radiative decay; intraband relaxation has no effect at this energy. The reason is that this detection energy lies very deep in the tail of the DOS, where the occurrence of neighboring segments with lower energy is negligible. For the detection at the peak position, we find a zero temperature decay time of 100 ps, which is about 16% faster than the purely radiative time scale of 120 ps at this energy. The difference is due to relaxation to lower lying exciton states in neighboring segments. Naturally, this effect is even stronger at the blue position, where the observed decay time of 44 ps is considerably faster than the purely radiative decay time of 168 ps. At this blue position, also an increased influence from intrasegment relaxation exists, as at these higher energies a fraction of the states already represent an excited segment state, with one node (Fig. 3).

We also observe from Fig. 8 that at high temperature the decay times for the different detection energies approach each other and in fact they then all tend to the decay time of the total fluorescence intensity [Fig. 7(b)]. This is a consequence of the fact that the scattering rates are then large enough for the exciton populations to become equilibrated

on the time scale of emission. A comparable observation was made in Ref. 19 for the decay of the populations of the various exciton states for homogeneous aggregates. We finally observe that the temperature dependence is nonmonotonic in the same temperature range for which the Stokes shift behaves nonmonotonically (Fig. 5). Indeed, we attribute this behavior to the same temperature activated intersegment relaxation via higher lying exciton states. At the blue detection side (which still lies in the red tail of the DOS), this effect leads to a decrease of the lifetime, as it opens extra decay channels. On the red side, the situation is more subtle. This energy is so deep in the red tail of the DOS, that even the activated migration hardly opens new channels for decay. Instead, the activated relaxation occurring at the blue side towards lower energies will lead to extra contributions in the fluorescence intensity at the red side and, thus, to a growth of the decay time at this energy. At the peak position, we deal with the intermediate situation and we see a very small net effect.

We notice that the general characteristics displayed in Fig. 8 very well cover the experimental results reported by Scheblykin *et al.*¹⁵

VI. SUMMARY AND CONCLUDING REMARKS

We have performed a numerical study of the temperature dependence of the exciton dynamics in linear Frenkel exciton systems with uncorrelated diagonal disorder. In particular, we have focused on the resulting temperature dependent steady-state fluorescence spectrum, its Stokes shift relative to the absorption spectrum, and the decay time of the total fluorescence intensity following pulsed excitation. The complicated exciton dynamics reflected in these observables is governed by the interplay between thermal redistribution of the excitons over a set of eigenstates, which are localized by the disorder, and their radiative emission. The redistribution of exciton population within the manifolds of localized exciton states was described by a Pauli master equation. The transition between two localized states was assumed to originate from the coupling of the excitons to acoustic phonons of the host medium, the transition rates being proportional to the overlap integral of the corresponding wave functions squared. The model is characterized by two free parameters, σ , which denotes the degree of disorder, and W_0 , the phonon-assisted exciton scattering rate, which sets the overall scale for transition rates between exciton states.

The fact that our model only accounts for scattering on acoustic phonons, in principle limits us to temperatures of the order of 100 K and less. This covers the temperature range of many experiments performed on linear dye aggregates. Besides, as is clear from our simulations, if the exciton scattering rate is large enough, equilibration within the exciton space (on the time scale for radiative dynamics) already occurs at temperatures below 100 K. Above the equilibration temperature, the precise nature of the scattering mechanism becomes unimportant. In practice, the fact that in our Pauli master equation for the exciton populations, homogeneous broadening (dephasing) cannot be considered, probably yields a stronger limitation to the accuracy at elevated temperatures than the restriction to acoustic phonons. Incorporating

dephasing, i.e., accounting for the possible breakdown of coherence within delocalization segments, requires considering the exciton density operator (also see end of Sec. IV A).

From our simulations we found that the Stokes shift of the fluorescence spectrum shows an anomalous (nonmonotonic) temperature dependence: it first increases upon increasing the temperature from zero, before, at a certain temperature, it starts to show the usual monotonic decrease. This behavior was found previously for disordered quantum wells and physically derives from thermal escape from local potential minima.²⁴ We have shown that for disordered chains, the details of this behavior and the temperature range over which the anomaly takes place can be understood from the specific features of the exciton energy spectrum in the vicinity of the lower band edge: it is formed of manifolds of states localized on well separated segments of the chain and higher states that are extended over several segments. The migration of excitons between different segments augmented via intermediate jumps to higher states, is responsible for the nonmonotonic behavior found in our simulations. Interestingly, such a nonmonotonic behavior of the Stokes shift has recently been observed for the linear aggregates of the cyanine dye THIATS in a glassy host.¹⁵

We also found that the temperature dependence of the decay time of the total fluorescence intensity is very sensitive to the initial excitation conditions. For broadband resonant excitation, the fluorescence decay time decreases upon increasing the temperature. The reason is that the initially created population of superradiant states is transferred to higher (dark) states. It is the time of this transfer that determines the fluorescence decay time. As this transfer time decreases with growing temperature, a decreasing fluorescence lifetime is found. Because fluorescence experiments are hard to perform under resonant excitation, it will be difficult to observe this effect of intraband redistribution in fluorescence. It would be of interest, however, to study its effect on resonantly excited photon echo experiments.⁴⁹

In the case of off-resonance blue-tail excitation (the condition that is usually met in fluorescence decay experiments), the fluorescence decay time goes up with growing temperature, showing a nearly linear growth after a low-temperature plateau. The extent of the plateau depends on both the absorption bandwidth and on the ratio of the rates for exciton hopping and radiative emission. This behavior, a decay time that grows with temperature, with a possible plateau at low temperatures, agrees with fluorescence experiments performed on the *J* bands of linear molecular aggregates. It is of particular interest to note that a nearly linear dependence has been observed for aggregates of BIC¹² and THIATS.¹⁴ Based on the density of states of homogeneous exciton systems, it has been suggested that such a linear dependence could only occur for two-dimensional systems.¹² It follows from our results that in the presence of disorder, a ubiquitous ingredient for molecular aggregates, one-dimensional exciton systems may exhibit such a linear temperature dependence as well. In Ref. 48, we showed that using the model analyzed in this article, it is possible to obtain good quantitative fits to the absorption spectrum, the temperature dependent Stokes

shift, as well as the temperature dependent fluorescence lifetime measured for aggregates of the dye THIATS.^{14,15}

ACKNOWLEDGMENTS

One of the authors (V.A.M.) acknowledges financial support through a NATO Fellowship and la Universidad Complutense for hospitality during the initial stage of this work.

¹For a recent overview see, e.g., *Semiconducting Polymers—Chemistry, Physics, and Engineering*, edited by G. Hadziioannou and P. van Hutten (VCH, Weinheim, 1999).

²A. Tilgner, H. P. Trommsdorff, J. M. Zeigler, and R. M. Hochstrasser, *J. Chem. Phys.* **96**, 781 (1992).

³*J-Aggregates*, edited by T. Kobayashi (World Scientific, Singapore, 1996).

⁴J. Knoester, in *Organic Nanostructures: Science and Application* (IOS, Amsterdam, 2002), pp. 149–186.

⁵S. de Boer and D. A. Wiersma, *Chem. Phys. Lett.* **165**, 45 (1990).

⁶H. Fidder, J. Knoester, and D. A. Wiersma, *Chem. Phys. Lett.* **171**, 529 (1990).

⁷H. Fidder, J. Knoester, and D. A. Wiersma, *J. Chem. Phys.* **95**, 7880 (1991).

⁸H. Fidder, J. Terpstra, and D. A. Wiersma, *J. Chem. Phys.* **94**, 6895 (1991).

⁹H. Fidder, Ph.D thesis, University of Groningen, 1993.

¹⁰H. Fidder and D. A. Wiersma, *Phys. Status Solidi B* **188**, 285 (1995).

¹¹J. Moll, S. Daehne, J. R. Durrant, and D. A. Wiersma, *J. Chem. Phys.* **102**, 6362 (1995).

¹²V. F. Kamalov, I. A. Struganova, and K. Yoshihara, *J. Phys. Chem.* **100**, 8640 (1996).

¹³E. O. Potma and D. A. Wiersma, *J. Chem. Phys.* **108**, 4894 (1998).

¹⁴I. G. Scheblykin, M. M. Bataiev, M. Van der Auweraer, and A. G. Vitukhnovsky, *Chem. Phys. Lett.* **316**, 37 (2000).

¹⁵I. G. Scheblykin, O. Yu. Sliusarenko, L. S. Lepnev, A. G. Vitukhnovsky, and M. Van der Auweraer, *J. Phys. Chem. B* **105**, 4636 (2001).

¹⁶F. C. Spano, J. R. Kuklinsky, and S. Mukamel, *Phys. Rev. Lett.* **65**, 211 (1990); *ibid.* *J. Chem. Phys.* **94**, 7534 (1991).

¹⁷V. A. Malyshev, *Opt. Spektrosk.* **71**, 873 (1991) [*Opt. Spectrosc.* **71**, 505 (1991)]; *J. Lumin.* **55**, 225 (1993).

¹⁸M. Bednarz, V. A. Malyshev, J. P. Lemaistre, and J. Knoester, *J. Lumin.* **94–95**, 271 (2001).

¹⁹M. Bednarz, V. A. Malyshev, and J. Knoester, *J. Chem. Phys.* **117**, 6200 (2002).

²⁰V. Chernyak, T. Meier, E. Tsiper, and S. Mukamel, *J. Phys. Chem. A* **103**, 10294 (1999).

²¹R. Kersting, U. Lemmer, R. F. Mahrt, K. Leo, H. Kurz, H. Bässler, and E. O. Göbel, *Phys. Rev. Lett.* **70**, 3820 (1993).

²²B. Mollay, U. Lemmer, R. Kersting, R. F. Mahrt, H. Kurz, H. F. Kauffmann, and H. Bässler, *Phys. Rev. B* **50**, 10769 (1994).

²³K. Brunner, A. Tortschanoff, Ch. Warmuth, H. Bässler, and H. F. Kauffmann, *J. Phys. Chem. B* **104**, 3781 (2000).

²⁴R. Zimmerman and E. Runge, *Phys. Status Solidi A* **164**, 511 (1997); M. Grassi Alessi *et al.*, *Phys. Rev. B* **61**, 10985 (2000).

²⁵H. Fidder, J. Knoester, and D. A. Wiersma, *J. Chem. Phys.* **98**, 6564 (1993).

²⁶J. R. Durrant, J. Knoester, and D. A. Wiersma, *Chem. Phys. Lett.* **222**, 450 (1994).

²⁷A. G. Vitukhnovsky, A. N. Lobanov, A. V. Pimenov, Y. Yonezawa, N. Kometani, K. Asumi, and J. Yano, *J. Lumin.* **87–89**, 260 (2000).

²⁸A. G. Vitukhnovsky, A. N. Lobanov, A. V. Pimenov, Y. Yonezawa, and N. Kometani, *Int. J. Mod. Phys. B* **15**, 4017 (2001).

²⁹L. D. Bakalis, I. Rubtsov, and J. Knoester, *J. Chem. Phys.* **117**, 5393 (2002).

³⁰M. Shimizu, S. Suto, and T. Goto, *J. Chem. Phys.* **114**, 2775 (2001).

³¹V. Malyshev and P. Moreno, *Phys. Rev. B* **51**, 14587 (1995).

³²Actually, small corrections to the sine wave functions of Eq. (2) due to the long-range dipole interactions change the factor $0.81(N+1)$ to $0.84(N+1)$ for N in the order of 100, see Ref. 7.

³³D. V. Makhov, V. V. Egorov, A. A. Bagatur'yants, and M. V. Alfimov, *Chem. Phys. Lett.* **245**, 371 (1995); *J. Chem. Phys.* **110**, 3196 (1999).

³⁴V. A. Malyshev, A. Rodríguez, and F. Domínguez-Adame, *Phys. Rev. B* **60**, 14140 (1999).

³⁵A. V. Malyshev and V. A. Malyshev, *Phys. Rev. B* **63**, 195111 (2001).

³⁶A. V. Malyshev and V. A. Malyshev, *J. Lumin.* **94–95**, 369 (2001).

³⁷M. Schreiber and Y. Toyozawa, *J. Phys. Soc. Jpn.* **51**, 1528 (1982); *ibid.* **51**, 1537 (1982).

³⁸L. D. Bakalis and J. Knoester, *J. Phys. Chem. B* **103**, 6620 (1999).

³⁹P. Dean, *Rev. Mod. Phys.* **44**, 127 (1972).

⁴⁰V. V. Ovsyankin, in *Spectroscopy of Solids Containing Rare-Earth Ions*, edited by A. A. Kaplyanskii and R. M. MacFarlane (North-Holland, Amsterdam, 1987), p. 343.

⁴¹A. S. Davydov, *Theory of Molecular Excitons* (Plenum, New York, 1971).

⁴²V. M. Agranovich and M. D. Galanin, in *Electronic Excitation Energy Transfer in Condensed Matter*, edited by V. M. Agranovich and A. A. Maradudin (North-Holland, Amsterdam, 1982).

⁴³L. D. Bakalis and J. Knoester, *J. Lumin.* **86–87**, 66 (2000).

⁴⁴T. Meier, V. Chernyak, and S. Mukamel, *J. Phys. Chem. B* **101**, 7332 (1997).

⁴⁵T. Renger, V. May, and O. Kühn, *Phys. Rep.* **343**, 138 (2001).

⁴⁶T. T. Basiev, V. A. Malyshev, and A. K. Przhevuskii, in *Spectroscopy of Solids Containing Rare-Earth Ions*, edited by A. A. Kaplyanskii and R. M. MacFarlane (North-Holland, Amsterdam, 1987), p. 275.

⁴⁷This type of exciton diffusion was recently suggested to explain the temperature-dependent trapping of excitons in linear molecular aggregates, see A. V. Malyshev, V. A. Malyshev, and F. Domínguez-Adame, *Chem. Phys. Lett.* **371**, 417 (2003); *J. Phys. Chem. B* **107**, 4418 (2003).

⁴⁸M. Bednarz, V. A. Malyshev, and J. Knoester, *Phys. Rev. Lett.* **91**, 217401 (2003).

⁴⁹S. de Boer, K. J. Vink, and D. A. Wiersma, *Chem. Phys. Lett.* **137**, 99 (1987).